Stanford Exploration Project, Report 112, November 11, 2002, pages 223–237

Modeling high-frequency acoustics velocities in patchy and partially saturated porous rock using differential effective medium theory

James G. Berryman[1]

ABSTRACT

Differential effective medium (DEM) theory is applied here to the problem of modeling physical properties of poroelastic media that are partially saturated with liquid. Typical fluid saturants are air and water, or gas and oil. If the liquid and gas saturants are homogeneously mixed, then we say the medium is partially saturated. If the liquid and gas saturants are poorly mixed, so each constituent occupies separate, but contiguous, regions of the porous medium, we say the medium has patchy saturation. Some examples are presented to show that a reasonable approach to modeling the effects of patchy saturation at high frequencies (200 kHz and above) is produced by treating the medium as if it is a composite of gas-saturated and liquid-saturated porous inclusions that are homogeneously mixed together. Estimates of the properties are obtained using differential effective medium theory. The results differ dramatically from those predicted by Gassmann's equations for homogeneous mixing of the fluids in individual pores. In particular, the shear modulus depends on the elastic properties of the fluid constituents, unlike the quasi-static behavior predicted by Gassmann.

INTRODUCTION

One of the perennial problems in rock physics has been the difficulty of understanding how seismic wave speeds in fluid saturated and partially fluid saturated rocks depend on the wave frequency. Field methods for exciting seismic waves are usually in the 1–100 Hz band, while well-logging tools might be in the 1–50 kHz band. However, the careful controlled experiments needed to verify the predictions of the theory can normally only be done at still higher frequencies, typically in the 200–1000 kHz band. This segmentation of the frequency band into its distinct regions of application has caused and continues to cause much confusion about what is known and unknown about wave propagation and attenuation in rocks.

Theoretical analyses of Gassmann (1951) and Biot (1956a,b) provide low frequency results. Gassmann's results in particular are very low frequency, really applicable to the quasi-static domain, and therefore strictly apply only to the very lowest seismic frequencies. But a skeptical scientist wants proof of these theories, and it is sometimes hard to find convincing

[1]**email:** berryman@sep.stanford.edu

verifications among experiments done on rocks. Plona (1980) provided one very nice series of ultrasound experiments ($\simeq$ 1 MHz) using water-saturated sintered glass-bead samples (instead of rocks) showing (Chin *et al.*, 1983) that the Biot-Gassmann theory is in fact correct even in this high frequency regime, at least for such simple porous materials. The likely reason for this success is the high permeability ($1 \sim 10$D) and lack of microcracks in the porous glass-bead samples.

Difficulties still exist in explaining some high frequency laboratory data, especially in situations having low fluid permeability (and therefore making it unlikely that Gassmann's quasi-static conditions are close to being satisfied) and also having partial saturation conditions (mixtures of gas and liquid are present in the pores). There has been extensive work on partial saturation by Nur and Simmons (1969), Domenico (1974), Walls (1982), Murphy (1984), Berryman *et al.* (1988), Endres and Knight (1989), Knight and Nolen-Hoeksema (1990), Dvorkin and Nur (1998), Dvorkin *et al.* (1999a,b), Johnson (2001), and Berryman *et al.* (2002a), among others. In particular, the work of Knight and Nolen-Hoeksema (1990) makes it particularly apparent that great care must be taken in modeling these types of materials because details clearly matter. Whether the gas and liquid components are homogeneously mixed or are distributed in a patchy manner (*i.e.*, gas here, liquid there) makes a significant difference in the measured wave speeds. Even for the shear waves, where according to Gassmann's low frequency calculations we might conclude that there should be no difference at all (Berryman, 1999), we find clearly observable differences at higher frequencies.

Through a series of recent publications (Berryman *et al.*, 2000; 2002a), it has become clear that the most appropriate of the simple effective medium models for partial saturation conditions at high frequencies is the differential effective medium (DEM) theory (Berryman *et al.*, 2002b). The present paper will show specifically how to use this theory to fit data on partial and patchy saturation in a low-porosity, low-permeability granite and two tight sandstones.

DIFFERENTIAL EFFECTIVE MEDIUM THEORY

Differential effective medium (DEM) theory (Bruggeman, 1935; Cleary *et al.*, 1980; Walsh, 1980; Norris, 1985; Avellaneda, 1987) takes the point of view that a composite material may be constructed by making infinitesimal changes in an already existing composite. There are only two effective medium schemes known at present that are realizable, *i.e.*, that have a definite microgeometry associated with the modeling scheme. The differential scheme is one of these (Cleary *et al.*, 1980; Norris, 1985; Avellaneda, 1987) — and one version of the self-consistent approach (Korringa *et al.*, 1979; Berryman, 1980a,b; Milton, 1985) is the other. This fact, together with the associated analytical capabilities (including ease of computation and flexibility of application), provides strong motivation to study the predictions of both of these schemes and the differential scheme in particular. We can have confidence that the results will always satisfy physical and mathematical constraints, such as the Hashin-Shtrikman bounds (Hashin and Shtrikman, 1961; 1962).

When the inclusions are sufficiently sparse that they do not form a single connected network throughout the composite, it is most appropriate to use the Differential Effective Medium

(DEM) to model their elastic behavior (Berge *et al.*, 1993). Assume that the host material has moduli K_m and μ_m, while the inclusion material has moduli K_i and μ_i. Then, the effective bulk and shear moduli (indicated as such by the asterisks) of the composite are parametrized by $K^*(y)$ and $\mu^*(y)$ where the volume fraction of the inclusion phase is y. The equations governing the changes in these constants are then well-known to be

$$(1-y)\frac{dK^*(y)}{dy} = \left[K_i - K^*(y)\right] P^{*i} \tag{1}$$

and

$$(1-y)\frac{d\mu^*(y)}{dy} = \left[\mu_i - \mu^*(y)\right] Q^{*i}, \tag{2}$$

where the scalar factors, P^{*i} and Q^{*i}, will be explained in the following paragraph, y is porosity which equals inclusion volume fraction here, and the subscript i again stands for inclusion phase. We assume that the reader is somewhat familiar with this approach, and will therefore not dwell on its derivation, which is easily found in many places including, for example, Berryman (1992). These equations are typically integrated starting from porosity $y = 0$ with values $K^*(0) = K_m$ and $\mu^*(0) = \mu_m$, which are assumed here for modeling purposes to be the mineral moduli values for the single homogeneous solid constituent. Integration then proceeds from $y = 0$ to the desired highest value $y = \phi$ (the porosity of the sample), or possibly over the whole range to $y = 1$ for some purposes of analysis. When integrating this way, we might imagine the result is, for example, simulating cracks being introduced slowly into a granite-like solid. The same procedure can be used for a sandstone-like material assuming this medium has starting porosity $y = \phi_0$ with $K^*(\phi_0) = K_s$ and $\mu^*(\phi_0) = \mu_s$. Integration then proceeds from $y = \phi_0$ to $y = 1$. This introduction of crack (or soft) porosity into a material containing spherical (or stiff) porosity is conceptually equivalent to the porosity distribution model of Mavko and Jizba (1991).

The factors P^{*i} and Q^{*i} appearing in (1) and (2) are the so-called polarization factors for bulk and shear modulus (Eshelby, 1957; Wu, 1966). These depend in general on the bulk and shear moduli of both the inclusion, the host medium (assumed to be the existing composite medium $*$ in DEM), and on the shapes of the inclusions. The polarization factors usually have been computed from Eshelby's well-known results (Eshelby, 1957) for ellipsoids, and Wu's work (Wu, 1966) on identifying the isotropically averaged tensor based on Eshelby's formulas. These results can be found in many places including Berryman (1980b) and Mavko *et al.* (1998).

Because it is relevant both to low porosity granites and to sandstones having equant (*i.e.*, close to spherical) porosity as well as flat cracks, the case we consider here is that of penny-shaped cracks, where

$$P^{*i} = \frac{K^* + \frac{4}{3}\mu_i}{K_i + \frac{4}{3}\mu_i + \pi\alpha\gamma^*} \tag{3}$$

and

$$Q^{*i} = \frac{1}{5}\left[1 + \frac{8\mu^*}{4\mu_i + \pi\alpha(\mu^* + 2\gamma^*)} + 2\frac{K_i + \frac{2}{3}(\mu_i + \mu^*)}{K_i + \frac{4}{3}\mu_i + \pi\alpha\gamma^*}\right], \tag{4}$$

with α ($0 < \alpha < 1$) being the crack (oblate spheroidal) aspect ratio,

$$\gamma^* \equiv \mu^*[(3K^* + \mu^*)/(3K^* + 4\mu^*)], \tag{5}$$

and where the superscript $*$ identifies constants of the matrix material when the inclusion volume fraction is y. This formula is a special limit of Eshelby's results not included in Wu's paper, but apparently first obtained by Walsh (1969). Walsh's derivation assumes $\mu_i/\mu_m << 1$ and allows $K_i/K_m << 1$, with these approximations being made before any assumptions about smallness of the aspect ratio α. By taking these approximations in the opposite order, *i.e.*, letting aspect ratio be small first and then making assumptions about smallness of the inclusion constants, we would obtain instead the commonly used approximation for disks. But this latter approximation is actually quite inappropriate for the bulk modulus when the inclusion phase is a gas such as air (for then the ratio $K_i/K_m << 1$) or for the shear modulus when the inclusion phase is any fluid (for then $\mu_i \equiv 0$), as the formulas become singular in these limits. This is why the penny-shaped crack model is commonly used instead for cracked rocks.

In general the DEM equations (1) and (2) are coupled, as both equations depend on both the bulk and shear modulus of the composite. This coupling is not a serious problem for numerical integration. Later in the paper, we will show results obtained from integrating the DEM equations numerically.

HIGH FREQUENCIES

Figure 1 displays data from one granite and two sandstones in the frequency range 200–1000 kHz (also see Table 1). These examples were chosen for common display to emphasize the fact that there can be very clear deviations from the Gassmann-Domenico predictions at high frequencies. In particular, we see the startling difference in the right-hand subplots (Figure 1b,d,f) that the slopes of the patchy saturation lines (*i.e.*, lines connecting data points for fully dry and fully saturated samples) in all three cases are negative, instead of positive as predicted for low-frequency behavior [see Berryman *et al.* (2002a)]. Nevertheless, all three plots on the left (Figure 1a,c,e) seem to behave in a manner consistent with the Gassmann-Domenico ideas. Sierra White granite and Schuler-Cotton Valley sandstone (both measured at about 200 kHz) show behavior consistent with our interpretation of nearly ideal patchy saturation, again consistent with the drainage method of producing the changes in saturation.

TABLE 1. Some physical parameters of the samples considered in Figure 1. (Note: 1 mD $\simeq 1 \times 10^{-15}$ m^2.)

Sample	*Porosity (%)*	*Permeability (mD)*	*Grain Size (μm)*
Sierra White granite[a]	0.8	–	–
Schuler-Cotton Valley sandstone[a]	3.3	1.1×10^{-3}	100
Spirit River sandstone[b]	5.2	1.0×10^{-3}	125–150

[a] Murphy (1982)
[b] Knight and Nolen-Hoeksema (1990); Murphy (1982); Walls (1982)

On the other hand, the Spirit River sandstone (Figures 1e,f) was measured in the 600 kHz to 1 MHz frequency range, and two distinct methods of saturation were employed. The drainage method in this case again seems to show patchy saturation content, although it is not very close to the ideal patchy saturation line. The imbibition data are expected to produce a more uniform distribution of gas and liquid in the pores than that obtainable in most cases with a drainage method. Thus, imbibition data should behave much as predicted by Gassmann-Domenico, at least at low frequencies. Here we observe in Figure 1e that the imbibition data do indeed mimic the predicted behavior of Gassmann-Domenico, even though we are at high frequencies. Taken together, these results seem to suggest that something fairly simple is happening to produce these data, and that the main issue in Figure 1b,d,f is probably the actual violation of the Gassmann's very low frequency result that the shear modulus is not influenced by the presence of the fluid, and/or how such behavior can be modelled.

Seifert *et al.*(1999), working at about 1 MHz, chose to use the symmetric effective medium theory of Berryman (1980a) to model their data. The frequencies used are low enough so that a typical wavelength is 2 mm, while the grain sizes for the sands studied range from 210 to 250 μm, so the wavelength is an order of magnitude larger than the grain sizes and effective medium theory can safely be used. For an unconsolidated sand fully saturated with liquid, such a system is fairly closely approximated by a fluid suspension and therefore the self-consistent scheme (Berryman, 1980a) is appropriate for their problem. However, it would not be appropriate for our partial saturation problem where the pore fluid is sometimes all gas, and the solid frame always plays the major role in supporting both compressional and shear stresses. The better choice for such problems is a differential effective medium (DEM) theory [see Berge *et al.* (1995) for a more complete discussion of the advantages and disadvantages of these methods]. Then the solid can be treated correctly as the host medium and the gas and liquid constituents are treated strictly as inclusion phases — a requirement for this problem.

Our calculation for patchy saturation first uses DEM to compute the bulk and shear moduli for a porous solid saturated with gas only, and then repeats the calculation for bulk and shear moduli for a porous solid saturated with liquid only. In both cases, the shear modulus starts out at the shear modulus of the solid host medium and this is gradually replaced by (zero) inclusion shear modulus as the final desired porosity is attained. Nevertheless, the results in the gas- and liquid-saturated cases differ in these calculations because even though they have the same value for inclusion shear modulus, they do not have the same value for inclusion bulk modulus. This difference is important to the computed results. The physical reason for the difference is that in a random medium when a shear stress is applied macroscopically, it is resolved microscopically into both shear and compressional component stresses [see Berryman and Wang (2001) for an analysis of this aspect of the problem]. Trapped liquid can support some of those resolved compressional stresses resulting from an applied shear stress and therefore makes the saturated porous medium stronger in both shear and compression than when the same medium is saturated instead with a gas. Thus, the theory shows that $\mu_{dr} \neq \mu_{sat}$ when the saturating fluid is a liquid. This result disagrees with Gassmann, but does not contradict Gassmann. The point is that Gassmann's result is quasi-static and therefore pertinent for much lower frequencies, wherein the fluid can respond to the applied shear field by simply moving out of the way. But for trapped fluids or relatively rapid wave propagation through the medium,

the result just described must hold.

At high enough frequencies, adding liquid to a partially saturated system will in fact increase the effective shear modulus of the system. Thus, when we plot λ/μ versus ρ/μ, it is no longer the case that ρ/μ is a monotonic function of saturation. The density ρ is still a monotonic increasing function of saturation S as before, but now μ is also a monotonic increasing function of saturation. Therefore, the ratio ρ/μ is not necessarily monotonic and its behavior depends on which of the competing changes in the numerator and denominator dominate. The results for Sierra White granite (very low porosity) in Figure 1b clearly show that the main effect of addition of liquid to the system is to produce changes in μ at low porosities, with the result that the patchy saturation line has the opposite sign of slope (seen in Figure 1b) as that predicted by Gassmann-Domenico (seen in Figure 1a) and the data tend to fall along this line. The results are similar but not quite so well behaved for the Schuler-Cotton Valley sandstone in Figure 1d.

The most interesting behavior is observed for the Spirit River sandstone in Figure 1f. Here we see very clearly that as the liquid saturation increases, at first we have an increase in ρ/μ and then, when some special value of saturation (near 40% for the drainage data) is achieved, the influence of liquid on the shear modulus becomes more important and dominates the remainder of the curves up to full saturation.

Of the examples shown here, all three deviate dramatically from the predicted Gassmann-Domenico behavior. All these cases have the lowest porosities and permeabilities of the examples considered by Berryman *et al.* (2002a). This effect is presumably related therefore to the influence of permeability on the inability of the pore fluid pressure to equilibrate during the passage time of the wave, *i.e.*, having a higher likelihood of acoustically disconnected porosity.

EXAMPLES

When modeling rocks using effective medium theory, or really any approach, it is important to minimize the number of choices (size and shape of the inclusions, etc.) available to the modeler. Especially when dealing with cracks and simultaneously with partial and patchy saturation, the number of possible scenarios multiplies rapidly. For example, it would be entirely realistic to assume that there is a distribution of both crack aspect ratios and sizes present in the rocks. But since this distribution is surely not known, we will assume instead that there is only a single aspect ratio of crack present and choose values to lie in the range $\alpha = 0.001$–0.1. The decision to have only one aspect ratio is arbitrary. But it is motivated by the need to minimize the nonuniqueness inherent in the enterprise of fitting these data. Occam's razor applies here: we try to use the simplest possible model (a single aspect ratio), and if we cannot fit the data then we have learned something about the rock. We will find however that the simplest model is always sufficient when fitting the velocity data alone. The range of values that are considered sensible are based in part on the data of Hadley (1976) on Westerly granite, where it was observed that α ranged from 10^{-4} all the way up to unity, with a mode around 10^{-3}.

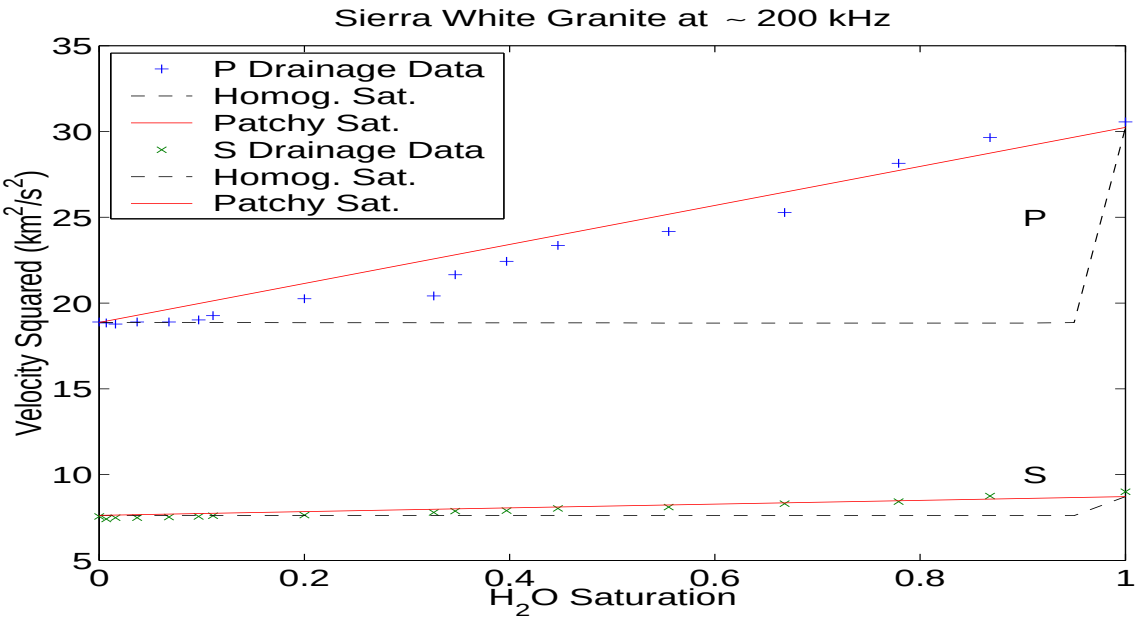

Figure 1: Square of the velocity data for the Sierra White granite measured by Murphy (1982) at 200 kHz. The dashed lines are the DEM results for compressional and shear when it is assumed that the saturation is homogeneous in each pore. The solid lines are the results for patchy saturation. Clearly, the data all fall closer to the patchy saturation lines at the higher values of liquid saturation. For the very lowest values of liquid saturation, the data seem to mimic the homogeneous saturation curve. jim1-swgvsq_all2 [NR]

Sierra White granite

All the data presented here for Sierra White granite are from Murphy (1982). This case is especially simple as the porosity is quite low ($\phi = 0.008$) and therefore the effect of liquid saturation on the density is very small ($< 0.3\%$ density effect), which we will treat for purposes of hand analysis as negligible. Thus, essentially the entire effect of liquid saturation depends on how the liquid is distributed in the pores and how this affects the bulk and shear moduli only. We will model this simply by considering the effects of gas saturation and liquid saturation separately and then combining the results [Voigt (1928) average] for the patchy saturation effects. For homogeneous saturation, we use DEM with an effective fluid bulk modulus given by the Reuss (1929) average (harmonic mean) of the fluids' moduli.

Murphy describes Sierra White as a granite "composed of a sparse population of low aspect ratio cracks, embedded in a composite of elastic grains." Some preliminary calculations done for the present work indicate that an aspect ratio of $\alpha \simeq 0.005$ to 0.02 should give results very consistent with the measured values for Sierra White. To fit the data at both the fully gas saturated end and the fully water saturated end, we found that $K_m = 57.7$ GPa and $\mu_m = 31.7$ GPa were good choices. The computation was performed at 21 equally spaced values of saturation for homogeneous saturation. The patchy saturation curve is obtained by connecting the two end points on a plot of velocity squared with a straight line. (For situations with

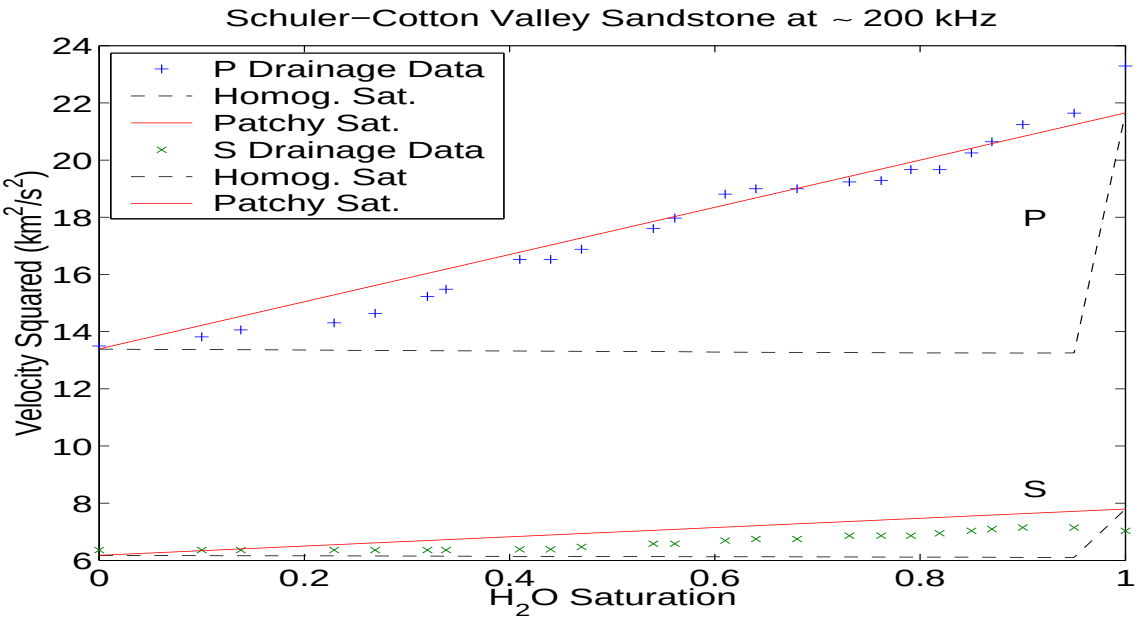

Figure 2: Square of the velocity data for the Schuler-Cotton Valley sandstone measured by Murphy (1982) at about 200 kHz. The dashed lines are the DEM results for compressional and shear when it is assumed that the saturation is homogeneous in each pore. The solid lines are the results for patchy saturation. In this case, all the data for compressional waves fall closer to the patchy saturation line than to the curve for homogeneous saturation. The data for shear waves seem to be much less sensitive to the assumed crack aspect ratio than were the compressional wave data. The results seem to suggest that the cracks that dominate compressional wave propagation are not the same as the ones dominating shear wave propagation for this sample. jim1-scvvsq_all2 [NR]

significant density variation, it is preferable to plot the Lamé constants λ and μ instead of the squares of the velocities — but for small porosity this is always a small difference that we choose to ignore here.) The results are shown in Figure 2. Clearly, all the data fall closer to the patchy saturation lines at the higher values of liquid saturation. For the very lowest values of liquid saturation, the data seem to mimic the homogeneous saturation curve, but at these low saturation levels the two curves are very close together anyway.

Schuler-Cotton Valley sandstone

The data presented here on Schuler-Cotton Valley sandstone are from Murphy (1982). Walls (1982) also studied permeability variations of other samples from the same formation, but both of his samples had higher porosity than the one studied by Murphy ($\phi = 0.033$). Murphy's compressional wave measurements were made at about 200 kHz and the shear measurements at about 150 kHz. The fitting parameters chosen for this sample were $K_m = 41.8$ GPa, $\mu_m = 36.7$ GPa, and $\alpha = 0.015$. Otherwise the analysis was identical to that for Sierra White granite. Results are shown in Figure 3. These curves are similar to those for the granite since the

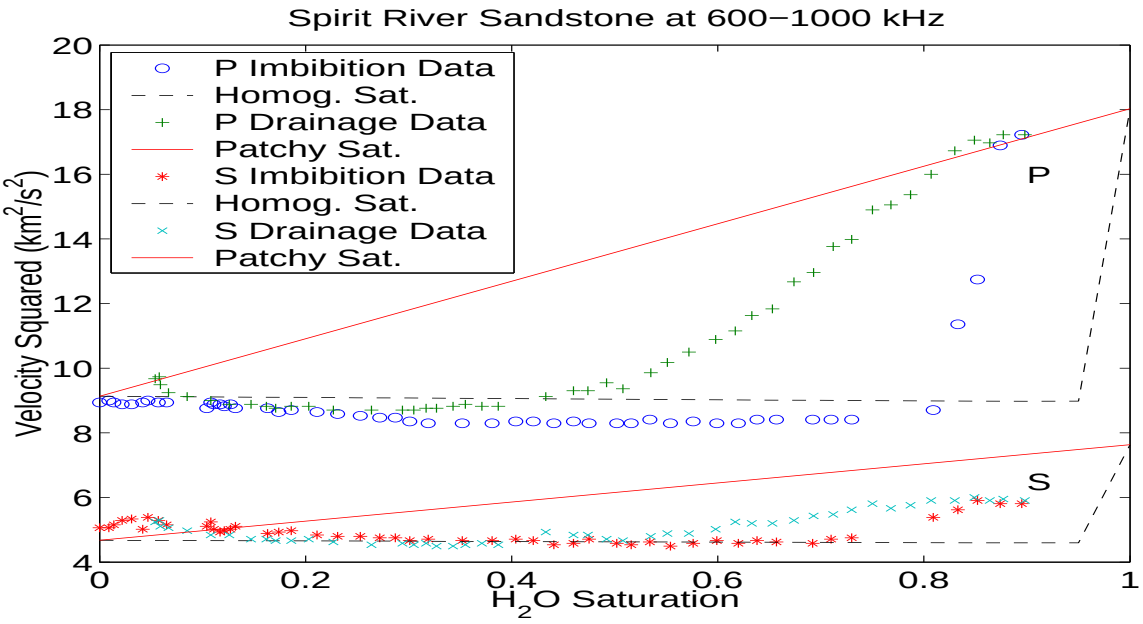

Figure 3: Square of the velocity data for the Spirit River sandstone measured by Knight and Nolen-Hoeksema (1990) in the range 600-1000 kHz. The dashed lines are the DEM results for compressional and shear when it is assumed that the saturation is homogeneous in each pore. The solid lines are the results for patchy saturation. Imbibition data are expected to fall closer to the homogeneous saturation curve, which is seen here for both V_p and V_s. Although the drainage data are expected to fall closer to the patchy saturation line, this tendency is only observed here at the higher saturation levels. See discussion in the text. jim1-srsvsq_all2 [NR]

compressional wave data show a very clear trend along the patchy saturation line. The shear wave data were harder to fit for this case, since the change in shear wave speed does not mimic that of the compressional wave as one might expect. For the Sierra White granite, a single value of α was sufficient to bring both P- and S-wave speeds into good agreement with the theoretical curves. Here, this was not possible, as the variation in compressional wave speed is substantially greater than that for the shear wave speed. A possible conclusion from this observed behavior is that the cracks that dominate compressional wave speed changes are not the same as those for the shear wave speed changes in this rock. But if this is true, it is not clear how to go about modeling such an effect.

Spirit River sandstone

The acoustical data on Spirit River sandstone are from Knight and Nolen-Hoeksema (1990). Both Murphy (1982) and Walls (1982) also studied the Spirit River sandstone, and Walls' sample SR6547 is apparently the same one studied by Knight and Nolen-Hoeksema. Imbibition data are expected to fall closer to the homogeneous saturation curve, which is seen to be true here for both V_p and V_s. Although the drainage data are expected to fall closer to the patchy

saturation line, this tendency is only observed here at the higher saturation levels (> 40 %).

Walls (1982) studied the gas permeability of the Spirit River sandstone as a function of both saturation and effective pressure. At room pressure the gas permeability changed from 100 μD to 47 μD as the liquid saturation changed from zero to 40%. Then, as the effective pressure increased, the permeability of the 40% saturated sample fell more rapidly than that of the other sample, differing by an order of magnitude at 30 MPa.

Since the porosity of this sample is about 5%, the volume fraction of the whole sample occupied by liquid at 40% saturation is about 2%. It is commonly observed that liquids can begin to percolate (*i.e.*, maintain a continuous connected pathway) across a porous sample when their volume fraction is of the order of 2-3%. So we assume that this dramatic departure of the observed drainage data is in some way related to this percolation threshold.

TABLE 2. Fitting parameters of the three rock samples considered in the text.

Sample	K_m (GPa)	μ_m (GPa)	α
Sierra White granite	57.7	31.7	0.005
Schuler-Cotton Valley sandstone	41.8	36.7	0.015
Spirit River sandstone	30.0	69.0	0.0125

Summary of results

The fitting parameters used to match the data in all three of the examples shown are listed in Table 2. For comparison, the values of bulk and shear moduli for quartz are often quoted as $K_m = 37.0$ GPa and $\mu_m = 44.0$ GPa, respectively. The fitting parameters obtained here lie in the ranges $30.0 \leq K_m \leq 57.7$ GPa and $31.7 \leq \mu_m \leq 69.0$ GPa. According to Walls (1982), the mineralogy of some other Schuler-Cotton Valley sandstones had about 72% quartz with the next most common mineral being quartz overgrowth ranging from 7-12%. The specific sample of Spirit River sandstone used by both Walls (192) and Knight and Nolen-Hoeksema (1990) had only about 34% quartz and 30% siderite, with the next most abundant components being chert, dolomite, and quartz overgrowth – each being in the range 7-10%. Siderite and dolomite both have significantly different, stronger bulk and shear moduli compared to quartz. So we conclude that the range of values observed in our fitting parameters are all quite possible, physically reasonable values but hard to check otherwise.

The observed grain sizes for Schuler-Cotton Valley sandstone and Spirit River sandstone were 100 μm and 125–150 μm, respectively. At the frequencies used in the experiments, the wavelengths for Schuler-Cotton Valley were $\lambda_p \simeq$ 18–24mm, and $\lambda_s \simeq$ 18mm. For Spirit River, the wavelengths were $\lambda_p \simeq$ 3–4mm and $\lambda_s \simeq$ 4mm. So, for Schuler-Cotton Valley, the grain size over wavelength is about 0.005, while, for Spirit River, it was about 0.035. We expect that the effective medium theory approach should be valid whenever these ratios are less than about 0.3, and certainly for an order of magnitude or more as is the case for these samples.

CONCLUSIONS

The main point of this exercise has been to show that the DEM equations are appropriate to use in this context (since the wavelengths are sufficiently long compared to the grain sizes) and that the DEM equations do in fact predict that right kinds of behavior in the high frequency range ($>$ 200 kHz). Gassmann's equations have clearly failed in this region (*i.e.*, the shear modulus is not independent of the fluid content), as would be expected. The quasi-static assumptions explicitly used in Gassmann's derivation are not satisfied in this frequency regime, and particularly so in rocks having low permeabilities (μD), as is the case for all the samples considered here. We can understand both qualitatively and semi-quantitatively what is happening in these samples by making use of DEM as a modeling tool. To do more detailed modeling requires much more detailed information about the constituents, their spatial distribution, their bonding characteristics, and the distribution and character of voids and cracks. We are still some ways from being able to determine all of these parameters in real rocks, but nevertheless can conclude that the methods described and used for modeling here do correctly capture the physics of these complicated high-frequency acoustics problems.

ACKNOWLEDGMENTS

I thank Bill Murphy and Rosemary Knight for providing access to their unpublished data files. I thank Pat Berge and Brian Bonner for helpful suggestions, and Morgan Brown for helpful comments that improved the manuscript.

REFERENCES

Avellaneda, M., 1987, Iterated homogenization, differential effective medium theory and applications: *Commun. Pure Appl. Math* **40**, 527–554.

Berge, P. A., Bonner, B. P., and Berryman, J. G., 1995, Ultrasonic velocity-porosity relationships for sandstone analogs made from fused glass beads: *Geophysics* **60**, 108–119.

Berryman, J. G., 1980a, Long-wavelength propagation in composite elastic media. I. Spherical inclusions: *J. Acoust. Soc. Am.* **68**, 1809–1819.

Berryman, J. G., 1980b, Long-wavelength propagation in composite elastic media II. Ellipsoidal inclusions: *J. Acoust. Soc. Am.* **68**, 1820–1831.

Berryman, J. G., 1992, Single-scattering approximations for coefficients in Biot's equations of poroelasticity: *J. Acoust. Soc. Am.* **91**, 551–571.

Berryman, J. G., 1999, Origin of Gassmann's equations: *Geophysics* **64**, 1627–1629.

Berryman, J. G., Berge, P. A., and Bonner, B. P., 2000, Transformation of seismic velocity data to extract porosity and saturation values for rocks: *J. Acoust. Soc. Am.* **107**, 3018–3027.

Berryman, J. G., Berge, P. A., and Bonner, B. P., 2002a, Estimating rock porosity and fluid saturation using only seismic velocities: *Geophysics* **67**, 391–404.

Berryman, J. G., Pride, S. R., and Wang, H. F., 2002b, A differential scheme for elastic properties of rocks with dry or saturated cracks: *Geophys. J. Int.*, accepted for publication in 2002.

Berryman, J. G., Thigpen, L., and Chin, R. C. Y., 1988, Bulk elastic wave propagation in partially saturated porous solids: *J. Acoust. Soc. Am.* **84**, 360–373.

Berryman, J. G, and Wang, H. F., 2001, Dispersion in poroelastic systems: *Phys. Rev. E* **64**, 011303-1–011303-16.

Biot, M. A., 1956a, Theory of propagation of elastic waves in a fluid-saturated porous solid. I. Low-frequency range: *J. Acoust. Soc. Am.* **28**, 168–178.

Biot, M. A., 1956b, Theory of propagation of elastic waves in a fluid-saturated porous solid. II. Higher frequency range: *J. Acoust. Soc. Am.* **28**, 179–1791.

Biot, M. A., 1962, Mechanics of deformation and acoustic propagation in porous media: *J. Appl. Phys.* **33**, 1482–1498.

Bruggeman, D. A. G., 1935, Berechnung verschiedener physikalischer Konstanten von heterogenen Substanzen: *Ann. Physik. (Leipzig)* **24**, 636–679.

Chin, R. C. Y., Berryman, J. G., and Hedstrom, G. W., 1985, Generalized ray expansion for pulse propagation and attenuation in fluid-saturated porous media: *Wave Motion* **7**, 43–66.

Cleary, M. P., Chen, I.-W., and Lee, S.-M., 1980, Self-consistent techniques for heterogeneous media: *ASCE J. Eng. Mech.* **106**, 861–887.

Domenico, S. N., 1974, Effect of water saturation on seismic reflectivity of sand reservoirs encased in shale: *Geophysics* **39**, 759–769.

Dvorkin, J., Mavko, G., and Nur, A., 1999a, Overpressure detection from compressional- and shear-wave data: *Geophys. Res. Lett.* **26**, 3417–3420.

Dvorkin, J., Moos, D., Packwood, J. L., and Nur, A. M., 1999b, Identifying patchy saturation from well logs: *Geophysics* **64**, 1756–1759.

Dvorkin, J. and Nur, A., 1998, Acoustic signatures of patchy saturation: *Int. J. Solids Struct.* **35**, 4803–4810.

Eshelby, J. D., 1957, The determination of the elastic field of an ellipsoidal inclusion, and related problems: *Proc. Roy. Soc. London A* **241**, 376–396.

Gassmann, F., 1951, Über die elastizität poröser medien: *Vierteljahrsschrift der Naturforschenden Gesellschaft in Zürich*, **96**, 1–23.

Hadley, K., 1976, Comparison of calculated and observed crack densities and seismic velocities in Westerly granite: *J. Geophys. Res.* **81**, 3484–3494.

Hashin, Z., and Shtrikman, S., 1961, Note on a variational approach to the theory of composite elastic materials: *J. Franklin Inst.* **271**, 336–341.

Hashin, Z., and Shtrikman, S., 1962, A variational approach to the theory of elastic behaviour of polycrystals: *J. Mech. Phys. Solids* **10**, 343–352.

Johnson, D. L., 2001, Theory of frequency dependent acoustics in patchy-saturated porous media: *J. Acoust. Soc. Am.* **110**, 682-694.

Knight, R., and Nolen-Hoeksema, R., 1990, A laboratory study of the dependence of elastic wave velocities on pore scale fluid distribution: *Geophys. Res. Lett.* **17**, 1529–1532.

Korringa, J., Brown, R. J. S., Thompson, D. D., and Runge, R. J., 1979, Self-consistent imbedding and the ellipsoidal model for porous rocks: *J. Geophys. Res.* **84**, 5591–5598 (1979).

Mavko, G., and Jizba, D., 1991, Estimating grain-scale fluid effects on velocity dispersion in rocks: *Geophysics* **56**, 1940–1949.

Mavko, G., Mukerji, T., and Dvorkin, J., 1998, *The Rock Physics Handbook: Tools for Seismic Analysis in Porous Media*, Cambridge University Press, Cambridge, pp. 307–309.

Milton, G. W., 1985, The coherent potential approximation is a realizable effective medium scheme: *Comm. Math. Phys.* **99**, 463–500.

Murphy, William F., III, 1982, *Effects of Microstructure and Pore Fluids on the Acoustic Properties of Granular Sedimentary Materials*, Ph.D. Dissertation, Stanford University.

Norris, A. N., 1985, A differential scheme for the effective moduli of composites: *Mech. Mater.* **4**, 1–16.

Nur, A., and Simmons, G., 1969, The effect of saturation on velocity in low porosity rocks: *Earth and Planet. Sci. Lett.* **7**, 183–193.

Plona, T. J., 1980, Observation of a second bulk compressional wave in a porous medium at ultrasonic frequencies: *Appl. Phys. Lett.* **36**, 259–261.

Reuss, A., 1929, Berechung der Fleissgrenze von Mischkristallen: *Z. Angew. Math. Mech.* **9**, 55.

Seifert, P. K., B. Kaelin, and L. R. Johnson, 1999, Effect on ultrasonic signals of viscous pore fluids in unconsolidated sand: *J. Acoust. Soc. Am.* **106**, 3089–3094.

Voigt, W., 1928, *Lehrbuch der Kristallphysik*, Teubner, Leipzig, p. 962.

Walls, J. D., 1982, Tight gas sands – permeability, pore structure: and clay: *J. Petroleum Technology* **34**, 2708–2714.

Walsh, J. B., 1965, The effect of cracks on the compressibility of rock: *J. Geophys. Res.* **70**, 381–389.

Walsh, J. B., 1980, Static deformation of rock: *ASCE J. Engng. Mech.* **106**, 1005–1019.

Wu, T. T., 1966, The effect of inclusion shape on the elastic moduli of a two-phase material: *Int. J. Solids Struct.* **2**, 1–8.